Influence of biomass burning plumes on HONO chemistry in eastern China

W. Nie[1,2], A. J. Ding[1,2,*], Y. N. Xie[1,2], Z. Xu[3], H. Mao[1,2,5], V.-M. Kerminen[4], L. F. Zheng[1,3], X. M. Qi[1,2], X. Huang[1,2], X. Q. Yang[1,2], J. N. Sun[1,2], E. Herrmann[1], T. Petäjä[4], M. Kulmala[4] and C. B. Fu[1,2]

[1]Institute for Climate and Global Change Research & School of Atmospheric Sciences, Nanjing University, Nanjing, 210093, China

[2]Colaborative Innovation Center of Climate Change, Jiangsu Province, China

[3] Environment Research Institute, Shandong University, Jinan, China

[4]Division of Atmospheric Sciences, Department of Physics, University of Helsinki, Helsinki, Finland

[5]Department of Chemistry, State University of New York College of Environmental Science and Forestry, Syracuse, New York, USA

*Correspondence to: A. J. Ding (dingaj@nju.edu.cn)

Abstract. Nitrous acid (HONO) plays a key role in atmospheric chemistry via influencing the budget of hydroxyl radical (OH). In this study, a two-month measurement of HONO and related quantities were analyzed during a biomass burning season in 2012 at a suburban site in the western Yangtze River Delta, eastern China. An overall high HONO concentration with the mean value of 0.76 ppbv (0.01 ppbv to 5.95 ppbv) was observed. During biomass burning (BB) periods, both HONO concentration and HONO/NO_2 ratio were enhanced significantly (more than a factor of 2, $p<0.01$) compared with non-biomass burning (Non-BB) periods. A correlation analysis showed that the HONO in BB plumes was more correlated with nitrogen dioxide (NO_2) than that with potassium (a tracer of BB). Estimation by the method of potassium tracer suggests a maximum contribution of 17% ± 12% from BB emission to the observed HONO concentrations, and the other over 80% of the observed

nighttime HONO concentrations during BB periods were secondarily produced by the heterogeneous conversion of NO_2. The NO_2-to-HONO conversion rate (C_{HONO}) in BB plumes was almost twice as that in non-BB plumes (0.0062 hr^{-1} vs 0.0032 hr^{-1}). Given the residence time of the BB air masses was lower than that of non-BB air masses, these results suggest BB aerosols have higher NO_2 conversion potentials to form HONO than non-BB aerosols. A further analysis based on comparing the surface area at similar particle mass levels and $HONO/NO_2$ ratios at similar surface area levels suggested larger specific surface areas and higher NO_2 conversion efficiencies of BB aerosols. A mixed plume of BB and anthropogenic fossil fuel (FF) emissions was observed on 10 June with even higher HONO concentrations and $HONO/NO_2$ ratios. The strong HONO production potential (high $HONO/NO_2$ to $PM_{2.5}$ ratio) was accompanied with a high sulfate concentration in this plume, suggesting a promotion of mixed aerosols to the HONO formation. In summary, our study suggests an important role of BB in atmospheric chemistry by affecting the HONO budget. This can be especially important in eastern China, where agricultural burning plumes are inevitably mixed with urban and industrial pollutions.

1. Introduction

Nitrous acid (HONO) is an important constituent in the troposphere due to its role in hydrogen oxides (HO_x) cycling (Platt et al., 1980; Kleffmann, 2007; Hofzumahaus et al., 2009; Elshorbany et al., 2012). The photolysis of HONO provides a daytime source of hydroxyl radical (OH), which controls the daytime oxidation capacity and consequently influences the ozone (O_3) chemistry and secondary organic aerosol (SOA) formation. This process is especially important in the early morning when contributions from other OH sources, like O_3 photolysis, are still small (Alicke et al., 2002; Kleffmann et al., 2005; Elshorbany et al., 2010).

The sources of atmospheric HONO, including direct emission from fossil fuel combustion (Kurtenbach et al., 2001) and soil (Su et al., 2011), homogeneous gas phase reactions and heterogeneous processes on the surface of atmospheric aerosols

and ground (Harrison and Collins, 1998; Longfellow et al., 1999; Stutz et al., 2002; VandenBoer et al., 2013), are hitherto not well understood. Among these sources, heterogeneous processes are commonly accepted as the least understood pathway to produce HONO. For example, nitrogen dioxide (NO_2) can be converted to HONO on ground (Harrison and Kitto, 1994), wet surfaces (Finlayson-Pitts et al., 2003), soot particles (Ammann et al., 1998; Kalberer et al., 1999; Kleffmann and Wiesen, 2005), and organic substrates (Bröske et al., 2003; Ammann et al., 2005). These processes have been considered as the primary contributor to the nocturnal HONO formation, but they cannot sustain the frequently-observed elevated daytime HONO concentration levels (Kleffmann, 2007; Sörgel et al., 2011; Li et al., 2012, and the references there in). Recently, several heterogeneous and possibly photo-enhanced processes have been demonstrated that might play an important role in daytime HONO formation (George et al., 2005; Stemmler et al., 2006; Ndour et al., 2008; Nie et al., 2012; Langridge et al., 2009; Bedjanian and El Zein, 2012). However, although these studies have drawn a clearer picture on the HONO chemistry, there are still large knowledge gaps in HONO sources. The heterogeneous production of HONO in the atmosphere by a variety of mechanisms is still under debate.

Biomass burning is a major source of atmospheric aerosol particles (Janhäll et al., 2010) and trace gases (Andreae and Merlet, 2001; Burling et al., 2010), consequently influencing climate and air quality. Recent studies have connected the HONO chemistry to biomass burning via both direct HONO emissions and emissions of soot particles (Roberts et al., 2010; Veres et al., 2010). Although high emission ratios of HONO have been detected in the laboratory fires (Burling et al., 2010; Veres et al., 2010), the mixing ratio of HONO in aged biomass burning plumes is expected to be relatively independent of its direct emissions due to the rapid dilution and photolysis for primary HONO during the atmospheric transport. Soot particles, as one major component in biomass burning plumes, have been demonstrated to be an effective media to convert NO_2 to HONO (Kleffmann et al., 1999; Aumont et al., 1999; Prince et al., 2002; Kleffmann and Wiesen, 2005; Aubin and Abbatt, 2007), especially in the

case that aged soot particles can be re-actived in the present of light (Monge et al., 2010) and play a continuous role in the HONO chemistry. These processes may significantly influence the HONO chemistry during a biomass burning period, but their exact roles are rarely demonstrated in the real atmosphere, especially when BB aerosols are mixed with anthropogenic pollutants.

In this study, a two-month measurement campaign was conducted during the intensive BB (burning of wheat straw) period (April to June 2012) at the SORPES station (Stations for Observing Regional Processes of the Earth System) in western Yangtze River Delta (YRD) of East China (Ding et al., 2013c). Several HONO-related quantities were measured, with the aim to investigate the HONO chemistry in YRD, a region undergoing rapid urbanization and industrialization. A special attention was paid to the impact of BB plumes and mixed plumes of agricultural burning and fossil fuel (FF) emissions on HONO formation after a long-range transport. In the following, the general features related to HONO during the campaign were first described. The differences in HONO formation between the BB events and non-BB events were then investigated. The influences of mixed plumes of intensive BB and FF emission (Ding et al., 2013b) on HONO formation were finally discussed.

2. Experimental methodologies

2.1 Field campaign

The field campaign was conducted from late April to June 2012 at the SORPES "flagship" central site in Xianlin of Nanjing (Ding et al., 2013c). It is a regional background site, located on the top of a hill (118°57'10" E, 32°07'14", 40 m a.s.l.) in the Xianlin campus of Nanjing University and about 20 km east of the suburban Nanjing city (See Fig. 1 in Ding et al., 2013c). A suite of trace gases, aerosols and meteorological quantities were measured, with more detailed descriptions found in Ding et al. (2013b). The present study is focused on HONO and related quantities, including NO_2, NO_x, CO, SO_2, $PM_{2.5}$ mass, total water-soluble ions (WSIs),

potassium ions (K^+), sulfate (SO_4^{2-}), and particle surface-area size distribution over the size range of 6–800 nm.

2.2 Measurement techniques

The HONO concentration was measured with a Monitor for Aerosols and Gases in Air (MARGA, Metrohm Co.), which includes a wet rotating denuder (WRD) (Spindler et al., 2003; Su et al., 2008; Makkonen et al., 2012) connected to an ion chromatograph (IC, Metrohm USA, Inc., Riverview, FL). The time resolution of this measurement is 1 h. There were 1608 hourly samples during the campaign. The WRD consists of two concentric glass cylinders whose wall is coated with 10 ppm H_2O_2 solution to absorb HONO and other gases. The liquid sample streams from WRD are drawn into 25 ml syringes before being injected into the IC system. The residence time of sampling air is about 4.5 s in the sampling tubes and about 0.2 s in WRD.

Other measurement techniques are described briefly as follows. The fine particle mass concentration ($PM_{2.5}$) was continuously measured with a combined technique of light scattering photometry and beta radiation attenuation (Thermo Scientific SHARP Monitor Model 5030). Sulfate (SO_4^{2-}) and potassium ions (K^+) concentrations in $PM_{2.5}$ were measured with the MARGA system (Ding et al., 2013b). NO_2 was converted to nitric oxide (NO) with a molybdenum oxide (MoO) catalytic converter inside the instrument and measured with a chemiluminescence analyzer (TEI model 42i). It should be noted that the technique of molybdenum converter to measure NO_2 may overestimate its ambient concentrations at daytime due to the potential conversion of species other than NO_2 (e.g. peroxyacetyl nitrate (PAN)) to NO (Xu et al., 2013). But the interference is much lower at nighttime without photochemical reaction. Total reactive nitrogen oxides (NO_y) was measured with an externally placed molybdenum converter and a NO analyzer. The sulfur dioxides (SO_2) concentration was measured with a pulsed UV fluorescence analyzer (TEI model 43i). Detailed information can be found in Ding et al. (2013c).

2.3 Sampling artifacts and data correction

The sampling artifacts of HONO measurement with WRD method are mainly caused by the NO_2 conversion on the surface of the sampling tube and WRD (interference 1) and the reaction of NO_2 with S (IV) in the absorption solution in WRD (interference 2) (Spindler et al., 2003; Barnes and Rudziński, 2012). In this study, 10 ppm of H_2O_2 was used as the absorption solution for the MARGA system, which can oxidize the S (IV) very quickly to form H_2SO_4, and thus can avoid the interference 2 induced by the reaction of NO_2 with S (IV) (Genfa et al., 2003). In addition, the formation of H_2SO_4 can acidify the absorption solution, which will reduce the interference 1 in WRD by suppressing the absorption and reaction of NO_2 on the surface of the absorption solution (Kleffmann et al., 2002). Therefore, in this study, the interference of HONO measurement should be mainly from the NO_2 conversion on the surface of the sampling tube (part of interference 1). Here, to avoid the possible overestimation, we corrected the dataset with the following formula recommended by an inter-comparison study on the HONO measurement between a WRD and a LOPAP system conducted in a similar atmospheric environment in China (Su, 2008):

$$HONO_{LOPAP}=0.833*HONO_{WRD}-0.17$$

It should be noted that the dataset corrected by this formula is expected to underestimate the HONO concentration because the absorption solution deployed by Su (2008) was Na_2CO_3, which can induce additional interference in WRD (interference 2 and part of interference 1). Given that we probably underestimated the HONO concentrations and overestimated the NO_2 concentrations (Xu et al., 2013), the values of $HONO/NO_2$ and $HONO/NO_x$ calculated in section 3 are actually lower limits for these ratios.

Several studies (Appel et al., 1990; Th. Muller, 1999; Genfa et al., 2003) have demonstrated that the overestimation of HONO concentrations measured by WRD are mainly occurred during daytime, so we used only nighttime data (except the case of 10 June, when the solar radiation was significantly decreased to a very low level (Ding et al., 2013b) in sections 3.2 and 3.3.

2.4 Calculation of the nocturnal HONO lifetime

Generally the nocturnal boundary layer is low and stable, the observed plumes during the nighttime were assumed to always be transported inside the boundary layer and probably contact to the ground surface. In this case, there are three major pathways for the loss of HONO during nighttime, including deposition on ground surfaces (Path-A), heterogeneous loss on aerosol surfaces (Path-B) and reaction with the OH radical (Path-C) (Li et al., 2012). For Path-A, the HONO lifetime (T_a) is given by

$$T_a = \frac{1}{k_a} = \frac{H}{V_{HONO}}$$

where H is the mixing height (assumed as 100 m) and V_{HONO} is the dry deposition velocity of HONO, assumed to be equal to 0.8 cm s^{-1} (Li et al., 2012). For the loss Path-B, the corresponding lifetime (T_b) can be written as

$$T_b = \frac{1}{k_b} = \frac{1}{\frac{1}{4} * \gamma_{HONO} S_{aerosol} * \overline{v_{HONO}}}$$

There is no modern literature reporting the HONO uptake coefficient on aerosol, but an uptake coefficient of HONO on the ground ranging from 10^{-5} to 10^{-4} was reported in recent studies (VandenBoer et al., 2013; Donaldson et al., 2013). Considering lower surface area and pH of aerosol (Su et al., 2011), the uptake coefficient of HONO on aerosol may be less and was estimated as 10^{-5} or less. $S_{aerosol}$ is the aerosol surface during the observation with a mean value of about 1.5×10^3 μm^2 cm^{-3} calculated from the particle size distribution, and $\overline{v_{HONO}}$ is the mean molecular velocity of HONO (about 380 m/s). For the loss Path-C, the lifetime (T_c) is equal to

$$T_c = \frac{1}{k_c} = \frac{1}{k * OH}$$

The OH concentration was estimated as 10^6 mol cm^{-3} (Hofzumahaus et al., 2009). $K_{HONO+OH}$ is the reaction rate of HONO and OH. The value of 5.0×10^{-12} cm^3 s^{-1} at 298 K (Sander et al., 2006) was used. In these conditions, the overall lifetime, $T_,$ is obtained from the following formula:

$$\frac{1}{T} = \frac{1}{T_a} + \frac{1}{T_b} + \frac{1}{T_c}$$

The lifetime of HONO was calculated to be about 3.3 hours. That means about 8-9 hours are needed to for the emitted HONO to be consumed within the nocturnal PBL.

2.5 Tracer of biomass burning plumes

Most BB tracers are organic compounds (Simoneit, 2002; Andreae and Merlet, 2001), which were not measured during this campaign. Carbon monoxide (CO) in the gas phase (Andreae and Merlet, 2001) and potassium ions (K^+) in the aerosol phase (ANDREAE, 1983; Ma et al., 2003; Reid et al., 2005; Li et al., 2007) are well recognized inorganic tracers of BB. In this study, the observation site is located in YRD, one of the best developed and most polluted regions in China (Ding et al., 2013c). Many CO sources other than BB, such as industry and traffic, can contribute a lot to the CO loading even during the BB season. Instead, no other significant sources of K^+ are around this region. Therefore, K^+ is suitable tracer of BB for the regions with heavy air pollutions. In this study, the samples with K^+ concentrations higher than 2 μg m^{-3} and the ratio of K^+ to $PM_{2.5}$ larger than 0.02 were defined as BB samples (203 samples). The samples with K^+ concentrations lower than 2 μg m^{-3} and the ratio of K^+ to $PM_{2.5}$ smaller than 0.02 were categorized as non-BB samples (1122 samples). The defined samples, including BB and non-BB samples, account for 82.4% of the total samples. The other undefined samples account for 17.6%.

3. Results and discussions

3.1 Observation overview

Figure 1 shows the temporal variations of concentrations of HONO, NO_2, $PM_{2.5}$ mass and K^+ observed at the Xianlin SORPES central site during the time period of April – June 2012. The average concentration of HONO was 0.76 ± 0.79 ppbv, which was lower than the concentrations measured at a polluted rural site in the Pearl River Delta region (Su et al., 2008) and an urban site in Shanghai (Wang et al., 2013), but much

higher than those measured in Europe (Acker and Möller, 2007). Both HONO concentrations (Fig. 2a) and ratios of HONO to NO_2 (HONO/NO_2) (Fig. 3b) exhibited distinct diurnal cycles, with a diurnal maximum during night/early morning and minimum around the noon.

During the campaign and especially from late May to early June, several BB episodes were observed and revealed by elevated concentrations of $PM_{2.5}$ (up to 426 μg m^{-3}) and K^+ (up to 22 μg m^{-3}) (Fig. 1) (Ding et al., 2013b; Ding et al., 2013c). HONO concentrations were also enhanced during the BB episodes. In order to investigate the relation between BB and HONO chemistry, we compared the HONO concentrations, HONO/NO_2 ratios and HONO/NO_x ratios between the BB and non-BB periods. On average, all the three parameters were significantly enhanced during BB periods than during non-BB periods (Figs. 3d-3f). HONO concentrations increased by 156% (1.56 ± 1.43 ppbv vs 0.61 ± 0.54 ppbv, $p<0.01$); HONO/NO_2 ratios increased by 137% (0.066 ± 0.043 vs 0.028 ± 0.020, $p<0.01$); HONO/NO_x ratios increased by 134% (0.055 ± 0.031 vs 0.023 ± 0.016, $p<0.01$). These results indicate a positive impact of BB plumes on the ambient mixing ratio of HONO.

The enhanced HONO production in BB plumes would impact the atmospheric oxidation capacity, and influence the formation of secondary aerosols (Li et al., 2010; Gonçalves et al., 2012; Elshorbany et al., 2014). In this study, the average values of HONO to NO_x ratios (0.028 ± 0.021), especially during the BB periods (0.062 ± 0.031) (see Fig. 3f) were considerably higher than 0.02, the assumed global averaged value (Elshorbany et al., 2012; Elshorbany et al., 2014), suggesting a potential more important role for HONO chemistry in the YRD, especially during the BB season.

3.2 Influence of BB on HONO formation

3.2.1 Contribution of direct emission

Several laboratory studies have demonstrated BB as an effective HONO source via direct emissions (Burling et al., 2010; Veres et al., 2010), so HONO might play an

important role in atmospheric chemistry over BB source regions. However, HONO is easily consumed by chemical sinks during its atmospheric transport (the estimated lifetime was about 3.3 hours in the night time, and emitted HONO can be consumed in about 8 hours, see section 2.4). In this study, the main BB source area is located in the northern part of Anhui province, several hundred kilometers from the SORPES station (Fig. 4). As showed in Fig. 4a, in addition to some individual fire points distributed in the 8-hr backward retroplume, the air masses from the major source regions cannot influence SORPES station in 8-hr transport, suggesting the direct emission from BB may influence on the observed enhancement of the HONO but should not be the major contributor. The correlations of HONO with K^+ (BB tracer) and NO_2 for the night time BB samples were illustrated in Fig. 5 and Fig.10. The results showed the HONO was positively correlated to both K^+ and NO_2, but the correlation efficiency (R) for HONO and NO_2 was higher than that for HONO and K^+. These results indicate that despite of some contribution from direction emission, the secondary production of HONO should play the key role.

As few publications reported the emission factors of both K^+ and HONO from the burning of wheat straw, here to estimate the contribution of BB direct emission to HONO, we first calculated the contribution of BB emission to observed CO concentrations. The ratio of emission factors of K^+ and CO was assumed to be identical for the BB events observed during this campaign. Here we took the minimum molar ratio of non-background CO to K^+ for night time BB samples (the value was 67) as the ratio of the emission factors of these two species because of the additional strong CO sources other than BB emission in YRD. The background concentrations of CO around SORPES station were estimated as the intercept of the linear regression fit for the whole samples of CO and NO_y during the campaign (the value was 480 ppb, figure not shown) (Wang et al., 2004). In such case, the CO concentration contributed from BB emission was calculated to be 260 ± 189 ppbv.

Then we estimated the contribution of BB emission to observed HONO concentrations by taking account of the emission ratio of HONO to CO from the

burning of wheat straw and the loss of emitted HONO during the transport. Noting that the deposition of CO and K^+ in fine particles was slow, their losses during the transport were assumed to be negligible. The averaged emission ratio of HONO to CO from the burning of wheat straw was taken as 0.0027 (Stockwell et al., 2014). The loss of HONO should be related to the transport time of BB plumes. However, the transport time was difficult to calculate as the exact source region (fire point on the map, Fig. 4) for each BB episode cannot be identified. Some episodes maybe influenced by several source regions on the transport pathway. And the exact time and duration of the fires cannot be identified with the satellite fire count data. But given that there were few fire points very close to SORPES station (Fig. 4), and the air plumes of several episodes, such as 9-11 June and 12-13 June, have been demonstrated being transported several days before arriving the station (Fig. 9d and 9e in Ding et al., 2013c), we therefore used 3.3 hours (HONO nighttime lifetime, see section 2.4) as the mean transport time, which is actually underestimated for most BB episodes to estimate HONO loss during transportation. In such case, although there may be large uncertainties, here our best estimation of HONO contribution from direct emission of BB was 0.27 $\pm$ 0.19 ppbv, which accounted for 17% $\pm$ 12% of the observed HONO concentrations. That means more than 80% of the observed nighttime HONO during BB periods was secondarily formed.

3.2.2 Heterogeneous conversion and possible influence of ground surface

Reaction of NO and OH was one major source of daytime HONO, but its contribution to nighttime HONO is negligible due to the limitation of nighttime OH concentration . Therefore, the over 80% of the observed HONO in the night time BB plumes, which was secondary formed, should be produced from the heterogeneous conversation of NO_2. In such case, the enhancement of HONO during BB periods should be ascribed to either the increase in NO_2 concentrations or increased NO_2 to HONO conversion potentials. As shown in Figs. 1 and 3c, the concentration levels of NO_2 were comparable during the BB and non-BB periods (p=0.51), so the higher HONO level during BB period was probably due in large part to a higher NO_2 conversion potential

285 (HONO/NO_2 ratio).

286 To further verify this point, in Fig. 6, we presented the changes of HONO to NO_2
287 ratios during night time for both BB and non-BB plumes. The NO_2-to-HONO
288 conversion rate (C_{HONO}), which estimated by change rates of HONO/NO_2 ratios along
289 the time (the slopes in Fig. 6, 19:00 to 03:00), in BB plumes almost 2 times higher
290 than that in non-BB plumes (0.0062 hr^{-1} vs 0.0032 hr^{-1}), further suggesting higher
291 NO_2 conversion potential to produce HONO in BB plumes than that in non-BB
292 plumes.

293 Both ground and aerosols are effective surfaces for converting NO_2 to HONO. Here,
294 to estimate the possible role of ground surface in the enhancement of HONO
295 concentrations, we conducted backward Lagrangian dispersion modeling for the air
296 masses arriving at the SORPES station using the HYSPLIT model following the
297 method developed by Ding et al., (2013a). Considering that the nighttime HONO
298 lifetime was estimated to be about 3.3 hours, we run the models for an 8-hour
299 backward period, during which the emitted HONO from BB can possibly be
300 consumed. Figs. 4a and 4b presented the "footprint" retroplumes, which represented
301 the distribution of probability or residence time of the simulated air masses in their
302 last 8-hour transport time prior to arrival at measurement site (Ding et al., 2013a). The
303 residence time was calculated to be 10% lower for BB air masses than that for
304 Non-BB air masses, suggesting the aerosol surface rather than the ground surface was
305 the major contributor to the observed enhancement of HONO concentrations and
306 HONO/NO_2 ratios during BB periods. It should be noted here we cannot totally get
307 rid of the influence of ground surface as the exact role of varied land use and land
308 cover in HONO chemistry was not clear. But the results tend to support the
309 heterogeneous reaction of NO_2 on the surface of BB aerosols were the major
310 contributors to the observed increase of HONO concentration during BB periods.

311 **3.2.3 Roles of BB aerosols in HONO chemistry**

312 The surface area and chemical nature of aerosol particles are the two dominating

factors that influence the heterogeneous conversion of NO_2 to produce HONO. In this study, the enhanced aerosol particle loadings associated with the BB plumes (Figs. 1 and 3a), providing large aerosol surface areas (Fig. 7a), should aid the conversion of NO_2 to HONO. Beside particle mass concentration, also the particle specific surface area related to the particle size distribution and morphology influences the total particle surface area concentration. In Fig. 7a, we present the relationship between the particle surface area and particle mass concentration ($PM_{2.5}$) for both the BB and non-BB samples. The slope of the data pairs for BB samples was almost twice as that of non-BB aerosols, suggesting a much higher specific surface area for BB aerosols than that for non-BB aerosols. To further verify this point and find out the causes, we selected the samples with the $PM_{2.5}$ mass in the overlap concentration range 100–150 μg m^{-3} during both BB and non-BB periods (Fig. 7a and 7b), and compared their surface area concentrations calculated by the size distribution (Fig. 7c). The results showed an evidently larger surface area concentration for BB aerosols compared with non-BB aerosols. These results clearly suggest that BB aerosols have a larger specific surface area than non-BB aerosol, which is caused by a much high number of accumulation mode particles, and favor NO_2 to HONO conversion at similar levels of the PM mass concentration. To further investigate the influence of BB aerosols on the particle specific surface area, we plotted the ratios of particle surface area to $PM_{2.5}$ against the abundance of potassium in $PM_{2.5}$ (Fig. 8) during BB periods. The result showed a positively linear correlation between the two metrics, suggesting a strong enhancement of BB aerosols on the particle specific area concentrations. Besides the surface area concentrations, the chemical nature of aerosols, which control the NO_2 conversion efficiency, is also a candidate influencing the transformation of NO_2 to HONO.

The NO_2 conversion efficiency refers to the ability of the interface to convert NO_2 to HONO. In the ambient air，both aerosol and ground surface contribute to the $HONO/NO_2$ ratio. Therefore, the NO_2 conversion efficiency can be represented by ($HONO/NO_2$) / (particle surface area + ground surface area) when the NO_2 and

HONO had reach a steady state (02:00-05:59, see Fig. 6). Here, we assume the related ground surface areas for each BB or non-BB sample are the same. In such case, the ratios of ($HONO/NO_2$) / (ground surface + aerosol surface) can only be compared when the aerosol surface areas of BB and non-BB aerosols were the same. Therefore, we selected the samples at HONO and NO_2 steady state with the surface area concentrations in the overlapped range 1.5–2.2 $\times 10^{-9}$ m^2 cm^{-3}, and compared the ratios of ($HONO/NO_2$) / (aerosol surface) to instead the comparison of ($HONO/NO_2$) / (ground surface + aerosol surface). As showed in Fig. 9, the values of this ratio were 67% higher for BB samples than those for non-BB samples, further suggesting the NO_2 conversion efficiency of BB aerosols was higher than that of Non-BB aerosols.

In summary, the elevated HONO formation observed in BB plumes was caused by the combined effects of enhanced particle loadings, higher specific aerosol surface areas, and more efficient conversion of NO_2 to HONO on particle surfaces. It is well known that high particle loadings associated with BB are caused by both primary particle emissions and secondary aerosol formation during the atmospheric transport (Andreae and Merlet, 2001; Li et al., 2003; Capes et al., 2008). Large aerosol specific surface areas are probably due to the extremely high number concentrations of accumulation mode particles during BB (Janhäll et al., 2010), and possibly the irregular shape of soot particles (Dobbins and Megaridis, 1987; Cai et al., 1993), which is one major product of BB. The higher NO_2 to HONO conversion efficiency on particle surfaces in BB plumes compared with non-BB air is a complex issue. One possible reason is the high abundance of organic (e.g. humic like substances) and soot particles (Reid et al., 2005), which are high-performance media to convert NO_2 to HONO. This is supported by the much higher concentrations of organics and black carbon, which were estimated as the differences of $PM_{2.5}$ and the water-soluble ions, in BB periods than those in Non-BB periods (see Fig. 3b).

3.3 Influence of mixed plume of biomass burning and fossil fuel emissions on HONO chemistry

An intense BB episode mixed with FF emissions that significantly influenced the everyday weather was observed on 10 June, 2012 (from 18:00 on 9 June to 05:00 on 11 June) (Ding et al., 2013b). Interestingly, the highest mixing ratios of HONO, exceeding 5 ppbv, occurred during this episode (Fig. 1). The solar radiation intensity was significantly decreased in the daytime of this episode due to the extremely high particle loading (See Fig. 3 in Ding et al., 2013b), and HONO concentrations during the daytime were at a similar level as those during the nighttime. Again, we investigated the relation between HONO and potassium. The result showed no correlation (slop=-0.08, R=0.24, figure not shown), suggesting that the enhanced HONO concentrations during the case of 10 June were secondarily produced. Although a high particle loading should be a contributor to the high HONO levels, it was not likely the most predominant factor because the PM concentrations during this event were comparable to the peak concentrations during the other BB episodes (Fig. 1). Another possible reason is that the plumes on 10 June were more aged than the other BB plumes, which would enhance the HONO production with a longer NO_2 contact time with aerosol and ground surface. However, as showed in Fig. 6, HONO and NO_2 can reach a steady state in 8 hours. The steady values of HONO/NO_2 ratios were 0.083 ± 0.014 (the value for 03:00) for other BB plumes, which were still much lower than those in June 10 case (0.17 ± 0.046), suggesting some other factors other than the plume age enhanced the HONO concentrations during 10 June.

Figure 10 shows the scatter plot between HONO and NO_2 concentrations during the BB periods. The dataset was separated into two groups: the first 5 hours of 10 June case (red squares, 18:00-22:00, on 9 June) combined with other BB episodes (blue squares) and later stage of the 10 June case (green circle dots). Both groups revealed a strong relation between HONO and NO_2 with a correlation coefficient higher than 0.8. The slope of the regression of the latter stage of the 10 June case was almost twice as that of the other group (0.12 vs 0.07), indicating a higher NO_2 to HONO conversion potential of the aerosols in the later stage of the 10 June case compared with other BB episodes.

To further verify this point and exclude the influence of particle loading, samples with $PM_{2.5}$ concentrations in range of 190–300 μg m^{-3} (the overlapping parts) were selected from both groups. Although the selected samples had similar PM concentration levels (Fig. 11a), the $HONO/NO_2$ ratios (Fig. 11b) and ratios between $HONO/NO_2$ and $PM_{2.5}$ (Fig. 11c) were much higher on 10 June than those during the other BB episodes, indicating a higher potential for the aerosols on 10 June to convert NO_2 to HONO. It should be noted that particle surface area data were not available for the 10 June case because the extremely high particle loading influenced the sample inlet of the DMPS. The exact contributors to the enhancement of NO_2 conversion potentials, which was either higher specific aerosol surface areas or stronger conversion efficiency, are therefore not clear.

Our previous study demonstrated that the episode on 10 June was caused by not only BB but a mixture of intense BB and anthropogenic FF emissions (Ding et al., 2013b). As shown in Fig. 12, the SO_2 concentration was low at the beginning of this episode and then gradually increased, suggesting the mixing of anthropogenic pollutions rich in SO_2 with the BB particles several hours after the invasion of the BB plume. This is why the chemical features ($HONO/NO_2$) in the plume of the beginning stage of the 10 June case was similar to that in other BB episodes, yet very different from the later stage of the 10 June case (Fig. 10).

The mix of BB plumes and FF emissions will promote the formation of secondary aerosols (e. g. sulfate and secondary organic aerosols (SOA)) on BB particles, and thus modify their morphology and surface chemical nature (Li et al., 2003; Capes et al., 2008). As shown in Fig. 11d, the abundance of sulfate in $PM_{2.5}$ was significantly enhanced in 10 June case compared with other BB episodes. This coincided with the high NO_2 to HONO conversion efficiency (Fig. 11c), indicating a promotion of secondary aerosol formation on BB particles in the mixed plumes to produce HONO. To further verify this point, we plotted the nighttime HONO concentration against the sulfate concentration on 10 June (Fig. 13), noting that the daytime HONO chemistry is completely out of the range of the nighttime correlations. The result shows a very

good correlation between the two compounds (R=0.79), further suggesting the promotion of secondary aerosol formation on BB particles to HONO formation.

As discussed above, the specific surface area and chemical nature of aerosol particles are the key factors in determining their potential to convert NO_2 to HONO. Therefore, changes in the morphology and size distribution caused by secondary aerosol formation may have enhanced the specific surface area and led to increased HONO production in the mixed plumes. Besides, the enhanced aerosol water content (Fig. 12) caused by the production of hydrophilic species, e.g. sulfate, may also play a role in accelerating the NO_2 conversion (Stutz et al., 2004). Another factor that might have enhanced HONO production could be the formation of some specific secondary material on BB particles, e.g. sulfate (Kleffmann et al., 1998) and secondary organic aerosols (Bröske et al., 2003).,

4. Conclusions and implications

In this study, we analyzed a two-month measurement of atmospheric HONO during the BB season of 2012 (May and June) at the SORPES station in western YRD of eastern China, and demonstrated an important role of BB in the HONO chemistry in the ambient atmosphere. Direct emissions from BB have been estimated to contribute 17% ± 12% of the observed HONO concentrations during nighttime BB episodes. The other over 80% was produced by the heterogeneous conversion of NO_2. The NO_2-to-HONO (C_{HONO}) conversion rates were detected to be significantly elevated during the BB periods due to the combined effect of enhanced particle loadings, larger specific surface areas of particles and higher NO_2 conversion efficiency on BB aerosols. An episode of mixed plumes of intense BB and anthropogenic FF emissions was observed on 10 June, during which the HONO production potentials from the conversion of NO_2 was further promoted by the formation of secondary particulate matter on BB particles.

Given that BB plumes are easily mixed with other anthropogenic pollutants in eastern

China, their influences on the atmospheric chemistry is expected to be important via affecting the HONO budget and thus the radical pool. Furthermore, considering the potential re-activation of BB particles (e.g. soot) during their atmospheric transport, the HONO chemistry associated with BB plumes may affect atmospheric chemistry long distances downwind BB areas, even in the marine boundary layer. Therefore, more studies are encouraged on BB related chemistry in eastern China, which is a unique "laboratory" with frequent mixed plumes of BB and anthropogenic pollutions.

Acknowledgements

This work was funded by National Natural Science Foundation of China (D0512/41305123 and D0510/41275129), the MOST 973 Program (2010CB428500), and the Jiangsu Provincial Science Fund for Distinguished Young Scholars (No. BK20140021). We thank T. Wang and L. Xue at The Hong Kong Polytechnic University for their suggestion on the data analysis. We are grateful of J. Kleffmann at Bergische Universität Wuppertal for his useful discussions on the data quality. We thank Metrohm Co. China for providing the MARGA analyzer and Z. Yan and J. Gao for their technical support for the instrument. We also thank the two anonymous referees and the editor for their construction and detailed comments during the review of this manuscript.

References

Acker, K., and Möller, D.: Atmospheric variation of nitrous acid at different sites in Europe, Environ. Chem., 4, 242-255, 10.1071/EN07023, 2007.

Alicke, B., Platt, U., and Stutz, J.: Impact of nitrous acid photolysis on the total hydroxyl radical budget during the Limitation of Oxidant Production/Pianura Padana Produzione di Ozono study in Milan, J. Geophys. Res.-Atmos., 107, 8196, 10.1029/2000JD000075, 2002.

Ammann, M., Kalberer, M., Jost, D. T., Tobler, L., Rössler, E., Piguet, D., Gäggeler, H. W., and Baltensperger, U.: Heterogeneous production of nitrous acid on soot in polluted air masses, Nature, 395, 157-160, 1998.

Ammann, M., Rössler, E., Strekowski, R., and George, C.: Nitrogen dioxide multiphase chemistry: Uptake kinetics on aqueous solutions containing phenolic compounds, Phys. Chem. Chem. Phys., 7, 2513-2518, 2005.

ANDREAE, M. O.: Soot Carbon and Excess Fine Potassium: Long-Range Transport of Combustion-Derived Aerosols, Science, 220, 1148-1151, 10.1126/science.220.4602.1148, 1983.

Andreae, M. O., and Merlet, P.: Emission of trace gases and aerosols from biomass burning, Global Biogeochem. Cy., 15, 955-966, 10.1029/2000gb001382, 2001.

Appel, B. R., Winer, A. M., Tokiwa, Y., and Biermann, H. W.: Comparison of atmospheric nitrous acid measurements by annular denuder and differential optical absorption systems, Atmos. Environ. Part A. General Topics, 24, 611-616, 10.1016/0960-1686(90)90016-G, 1990.

Aubin, D. G., and Abbatt, J. P. D.: Interaction of NO_2 with Hydrocarbon Soot: Focus on HONO Yield, Surface Modification, and Mechanism, J. Phys. Chem. A, 111, 6263-6273, 10.1021/jp068884h, 2007.

Aumont, B., Madronich, S., Ammann, M., Kalberer, M., Baltensperger, U., Hauglustaine, D., and Brocheton, F.: On the NO_2 + soot reaction in the atmosphere, J. Geophys. Res.-Atmos., 104, 1729-1736, 10.1029/1998jd100023, 1999.

Barnes, I., and Rudziński, K. J.: Disposal of Dangerous Chemicals in Urban Areas and Mega Cities-Role of Oxides and Acids of Nitrogen in Atmospheric Chemistry, Springer, 2012.

Bedjanian, Y., and El Zein, A.: Interaction of NO_2 with TiO_2 Surface Under UV Irradiation: Products Study, J. Phys. Chem. A, 116, 1758-1764, 10.1021/jp210078b, 2012.

Bröske, R., Kleffmann, J., and Wiesen, P.: Heterogeneous conversion of NO_2 on secondary organic aerosol surfaces: A possible source of nitrous acid (HONO) in the atmosphere?, Atmos. Chem. Phys., 3, 469-474, 10.5194/acp-3-469-2003, 2003.

Burling, I. R., Yokelson, R. J., Griffith, D. W. T., Johnson, T. J., Veres, P., Roberts, J. M., Warneke, C., Urbanski, S. P., Reardon, J., Weise, D. R., Hao, W. M., and de Gouw, J.: Laboratory measurements of trace gas emissions from biomass burning of fuel types from the southeastern and southwestern United States, Atmos. Chem. Phys., 10, 11115-11130, 10.5194/acp-10-11115-2010, 2010.

Cai, J., Lu, N., and Sorensen, C. M.: Comparison of size and morphology of soot aggregates as determined by light scattering and electron microscope analysis, Langmuir, 9, 2861-2867, 10.1021/la00035a023, 1993.

Capes, G., Johnson, B., McFiggans, G., Williams, P. I., Haywood, J., and Coe, H.: Aging of biomass burning aerosols over West Africa: Aircraft measurements of chemical composition, microphysical properties, and emission ratios, J. Geophys. Res.-Atmos., 113, D00C15, 10.1029/2008JD009845, 2008.

Ding, A. J., Wang, T., and Fu, C. B.: Transport characteristics and origins of carbon monoxide and ozone in Hong Kong, South China, J. Geophys. Res.-Atmos., 118, 9475-9488, 10.1002/jgrd.50714, 2013a.

Ding, A. J., Fu, C. B., Yang, X. Q., Sun, J. N., Petäjä, T., Kerminen, V. M., Wang, T., Xie, Y., Herrmann, E., Zheng, L. F., Nie, W., Liu, Q., Wei, X. L., and Kulmala, M.: Intense atmospheric pollution modifies weather: a case of mixed biomass burning with fossil fuel combustion pollution in eastern China, Atmos. Chem. Phys., 13, 10545-10554, 10.5194/acp-13-10545-2013, 2013b.

Ding, A. J., Fu, C. B., Yang, X. Q., Sun, J. N., Zheng, L. F., Xie, Y. N., Herrmann, E., Nie,

W., Petäjä, T., Kerminen, V. M., and Kulmala, M.: Ozone and fine particle in the western Yangtze River Delta: an overview of 1 yr data at the SORPES station, Atmos. Chem. Phys., 13, 5813-5830, 10.5194/acp-13-5813-2013, 2013c.

Dobbins, R. A., and Megaridis, C. M.: Morphology of flame-generated soot as determined by thermophoretic sampling, Langmuir, 3, 254-259, 1987.

Donaldson, M. A., Berke, A. E., and Raff, J. D.: Uptake of Gas Phase Nitrous Acid onto Boundary Layer Soil Surfaces, Environ. Sci. Technol., 48, 375-383, 10.1021/es404156a, 2013.

Elshorbany, Y., Barnes, I., Becker, K. H., Kleffmann, J., and Wiesen, P.: Sources and cycling of tropospheric hydroxyl radicals—an overview, Int. J. Res. Phys. Chem. Chem. Phys, 2010.

Elshorbany, Y. F., Steil, B., Brühl, C., and Lelieveld, J.: Impact of HONO on global atmospheric chemistry calculated with an empirical parameterization in the EMAC model, Atmos. Chem. Phys., 12, 9977-10000, 10.5194/acp-12-9977-2012, 2012.

Elshorbany, Y. F., Crutzen, P. J., Steil, B., Pozzer, A., Tost, H., and Lelieveld, J.: Global and regional impacts of HONO on the chemical composition of clouds and aerosols, Atmos. Chem. Phys., 14, 1167-1184, 10.5194/acp-14-1167-2014, 2014.

Genfa, Z., Slanina, S., Brad Boring, C., Jongejan, P. A. C., and Dasgupta, P. K.: Continuous wet denuder measurements of atmospheric nitric and nitrous acids during the 1999 Atlanta Supersite, Atmos. Environ., 37, 1351-1364, 10.1016/S1352-2310(02)01011-7, 2003.

George, C., Strekowski, R. S., Kleffmann, J., Stemmler, K., and Ammann, M.: Photoenhanced uptake of gaseous NO_2 on solid organic compounds: a photochemical source of HONO?, Faraday Discuss., 130, 195-210, 10.1039/b417888m, 2005.

Gonçalves, M., Dabdub, D., Chang, W. L., Jorba, O., and Baldasano, J. M.: Impact of HONO sources on the performance of mesoscale air quality models, Atmos. Environ., 54, 168-176, 10.1016/j.atmosenv.2012.02.079, 2012.

Harrison, R. M., and Collins, G. M.: Measurements of Reaction Coefficients of NO_2 and

HONO on Aerosol Particles, J. Atmos. Chem., 30, 397-406, 10.1023/a:1006094304069, 1998.

Harrison, R. M., and Kitto, A.-M. N.: Evidence for a surface source of atmospheric nitrous acid, Atmos. Environ., 28, 1089-1094, 10.1016/1352-2310(94)90286-0, 1994.

Hofzumahaus, A., Rohrer, F., Lu, K., Bohn, B., Brauers, T., Chang, C.-C., Fuchs, H., Holland, F., Kita, K., Kondo, Y., Li, X., Lou, S., Shao, M., Zeng, L., Wahner, A., and Zhang, Y.: Amplified Trace Gas Removal in the Troposphere, Science, 324, 1702-1704, 10.1126/science.1164566, 2009.

Janhäll, S., Andreae, M. O., and Pöschl, U.: Biomass burning aerosol emissions from vegetation fires: particle number and mass emission factors and size distributions, Atmos. Chem. Phys., 10, 1427-1439, 10.5194/acp-10-1427-2010, 2010.

Kalberer, M., Ammann, M., Arens, F., Gäggeler, H. W., and Baltensperger, U.: Heterogeneous formation of nitrous acid (HONO) on soot aerosol particles, J. Geophys. Res.-Atmos., 104, 13825-13832, 10.1029/1999jd900141, 1999.

Kleffmann, J., Becker, K. H., and Wiesen, P.: Heterogeneous NO_2 conversion processes on acid surfaces: possible atmospheric implications, Atmos. Environ., 32, 2721-2729, 10.1016/S1352-2310(98)00065-X, 1998.

Kleffmann, J., Becker, K. H., Lackhoff, M., and Wiesen, P.: Heterogeneous conversion of NO_2 on carbonaceous surfaces, Phys. Chem. Chem. Phys., 1, 5443-5450, 10.1039/a905545b, 1999.

Kleffmann, J., Heland, J., Kurtenbach, R., Lorzer, J., and Wiesen, P.: A new instrument (LOPAP) for the detection of nitrous acid (HONO), Environ. Sci. Pollut. R., 48-54, 2002.

Kleffmann, J., Gavriloaiei, T., Hofzumahaus, A., Holland, F., Koppmann, R., Rupp, L., Schlosser, E., Siese, M., and Wahner, A.: Daytime formation of nitrous acid: A major source of OH radicals in a forest, Geophys. Res. Lett., 32, L05818, 10.1029/2005GL022524, 2005.

Kleffmann, J., and Wiesen, P.: Heterogeneous conversion of NO_2 and NO on HNO_3 treated

586 soot surfaces: atmospheric implications, Atmos. Chem. Phys., 5, 77-83,
587 10.5194/acp-5-77-2005, 2005.
588 Kleffmann, J.: Daytime Sources of Nitrous Acid (HONO) in the Atmospheric Boundary
589 Layer, ChemPhysChem, 8, 1137-1144, 10.1002/cphc.200700016, 2007.
590 Kurtenbach, R., Becker, K. H., Gomes, J. A. G., Kleffmann, J., Lörzer, J. C., Spittler, M.,
591 Wiesen, P., Ackermann, R., Geyer, A., and Platt, U.: Investigations of emissions and
592 heterogeneous formation of HONO in a road traffic tunnel, Atmos. Environ., 35,
593 3385-3394, 10.1016/S1352-2310(01)00138-8, 2001.
594 Langridge, J. M., Gustafsson, R. J., Griffiths, P. T., Cox, R. A., Lambert, R. M., and Jones, R.
595 L.: Solar driven nitrous acid formation on building material surfaces containing titanium
596 dioxide: A concern for air quality in urban areas?, Atmos. Environ., 43, 5128-5131,
597 10.1016/j.atmosenv.2009.06.046, 2009.
598 Li, G., Lei, W., Zavala, M., Volkamer, R., Dusanter, S., Stevens, P., and Molina, L. T.:
599 Impacts of HONO sources on the photochemistry in Mexico City during the
600 MCMA-2006/MILAGO Campaign, Atmos. Chem. Phys., 10, 6551-6567,
601 10.5194/acp-10-6551-2010, 2010.
602 Li, J., Pósfai, M., Hobbs, P. V., and Buseck, P. R.: Individual aerosol particles from biomass
603 burning in southern Africa: 2, Compositions and aging of inorganic particles, J. Geophys.
604 Res.-Atmos., 108, 8484, 10.1029/2002JD002310, 2003.
605 Li, X., Wang, S., Duan, L., Hao, J., Li, C., Chen, Y., and Yang, L.: Particulate and Trace Gas
606 Emissions from Open Burning of Wheat Straw and Corn Stover in China, Environ. Sci.
607 Technol., 41, 6052-6058, 10.1021/es0705137, 2007.
608 Li, X., Brauers, T., Häseler, R., Bohn, B., Fuchs, H., Hofzumahaus, A., Holland, F., Lou, S.,
609 Lu, K. D., Rohrer, F., Hu, M., Zeng, L. M., Zhang, Y. H., Garland, R. M., Su, H., Nowak,
610 A., Wiedensohler, A., Takegawa, N., Shao, M., and Wahner, A.: Exploring the
611 atmospheric chemistry of nitrous acid (HONO) at a rural site in Southern China, Atmos.
612 Chem. Phys., 12, 1497-1513, 10.5194/acp-12-1497-2012, 2012.
613 Longfellow, C. A., Ravishankara, A. R., and Hanson, D. R.: Reactive uptake on hydrocarbon

soot: Focus on NO_2, J. Geophys. Res.-Atmos., 104, 13833-13840, 10.1029/1999jd900145, 1999.

Ma, Y., Weber, R. J., Lee, Y. -N., Orsini, D. A., Maxwell-Meier, K., Thornton, D. C., Bandy, A. R., Clarke, A. D., Blake, D. R., Sachse, G. W., Fuelberg, H. E., Kiley, C. M., Woo, J. -H., Streets, D. G., and Carmichael, G. R.: Characteristics and influence of biosmoke on the fine-particle ionic composition measured in Asian outflow during the Transport and Chemical Evolution Over the Pacific (TRACE-P) experiment, J. Geophys. Res.-Atmos., 108, 8816, 10.1029/2002JD003128, 2003.

Makkonen, U., Virkkula, A., Mäntykenttä, J., Hakola, H., Keronen, P., Vakkari, V., and Aalto, P. P.: Semi-continuous gas and inorganic aerosol measurements at a Finnish urban site: comparisons with filters, nitrogen in aerosol and gas phases, and aerosol acidity, Atmos. Chem. Phys., 12, 5617-5631, 10.5194/acp-12-5617-2012, 2012.

Monge, M. E., D'Anna, B., Mazri, L., Giroir-Fendler, A., Ammann, M., Donaldson, D. J., and George, C.: Light changes the atmospheric reactivity of soot, P. Natl. Acad. Sci. USA, 107, 6605-6609, 10.1073/pnas.0908341107, 2010.

Ndour, M., D'Anna, B., George, C., Ka, O., Balkanski, Y., Kleffmann, J., Stemmler, K., and Ammann, M.: Photoenhanced uptake of NO_2 on mineral dust: Laboratory experiments and model simulations, Geophys. Res. Lett., 35, L05812, 10.1029/2007gl032006, 2008.

Nie, W., Wang, T., Xue, L. K., Ding, A. J., Wang, X. F., Gao, X. M., Xu, Z., Yu, Y. C., Yuan, C., Zhou, Z. S., Gao, R., Liu, X. H., Wang, Y., Fan, S. J., Poon, S., Zhang, Q. Z., and Wang, W. X.: Asian dust storm observed at a rural mountain site in southern China: chemical evolution and heterogeneous photochemistry, Atmos. Chem. Phys., 12, 11985-11995, 10.5194/acp-12-11985-2012, 2012.

Platt, U., Perner, D., Harris, G. W., Winer, A. M., and Pitts, J. N.: Observations of nitrous acid in an urban atmosphere by differential optical absorption, Nature, 285, 312- 314, doi:10.1038/285312a0, 1980.

Prince, A. P., Wade, J. L., Grassian, V. H., Kleiber, P. D., and Young, M. A.: Heterogeneous reactions of soot aerosols with nitrogen dioxide and nitric acid: atmospheric chamber and Knudsen cell studies, Atmos. Environ., 36, 5729-5740,

643 10.1016/S1352-2310(02)00626-X, 2002.

644 Reid, J. S., Koppmann, R., Eck, T. F., and Eleuterio, D. P.: A review of biomass burning
645 emissions part II: intensive physical properties of biomass burning particles, Atmos.
646 Chem. Phys., 5, 799-825, 10.5194/acp-5-799-2005, 2005.

647 Roberts, J. M., Veres, P., Warneke, C., Neuman, J. A., Washenfelder, R. A., Brown, S. S.,
648 Baasandorj, M., Burkholder, J. B., Burling, I. R., Johnson, T. J., Yokelson, R. J., and de
649 Gouw, J.: Measurement of HONO, HNCO, and other inorganic acids by negative-ion
650 proton-transfer chemical-ionization mass spectrometry (NI-PT-CIMS): application to
651 biomass burning emissions, Atmos. Meas. Tech., 3, 981-990, 10.5194/amt-3-981-2010,
652 2010.

653 Sörgel, M., Regelin, E., Bozem, H., Diesch, J. M., Drewnick, F., Fischer, H., Harder, H., Held,
654 A., Hosaynali-Beygi, Z., Martinez, M., and Zetzsch, C.: Quantification of the unknown
655 HONO daytime source and its relation to NO_2, Atmos. Chem. Phys., 11, 10433-10447,
656 10.5194/acp-11-10433-2011, 2011.

657 Sander, S. P., Golden, D., Kurylo, M., Moortgat, G., Wine, P., Ravishankara, A., Kolb, C.,
658 Molina, M., Finlayson-Pitts, B., and Huie, R.: Chemical kinetics and photochemical data
659 for use in atmospheric studies evaluation number 15, 2006.

660 Simoneit, B. R. T.: Biomass burning — a review of organic tracers for smoke from
661 incomplete combustion, Appl. Geochem., 17, 129-162, 10.1016/S0883-2927(01)00061-0,
662 2002.

663 Spindler, G., Hesper, J., Brüggemann, E., Dubois, R., Müller, Th., and Herrmann, H.: Wet
664 annular denuder measurements of nitrous acid: laboratory study of the artefact reaction
665 of NO_2 with S(IV) in aqueous solution and comparison with field measurements, Atmos.
666 Environ., 37, 2643-2662, 10.1016/S1352-2310(03)00209-7, 2003.

667 Stemmler, K., Ammann, M., Donders, C., Kleffmann, J., and George, C.: Photosensitized
668 reduction of nitrogen dioxide on humic acid as a source of nitrous acid, Nature, 440,
669 195-198, 2006.

670 Stockwell, C. E., Yokelson, R. J., Kreidenweis, S. M., Robinson, A. L., DeMott, P. J.,

671 Sullivan, R. C., Reardon, J., Ryan, K. C., Griffith, D. W. T., and Stevens, L.: Trace gas
672 emissions from combustion of peat, crop residue, domestic biofuels, grasses, and other
673 fuels: configuration and Fourier transform infrared (FTIR) component of the fourth Fire
674 Lab at Missoula Experiment (FLAME-4), Atmos. Chem. Phys., 14, 9727-9754,
675 10.5194/acp-14-9727-2014, 2014.
676 Stutz, J., Alicke, B., and Neftel, A.: Nitrous acid formation in the urban atmosphere: Gradient
677 measurements of NO_2 and HONO over grass in Milan, Italy, J. Geophys. Res.-Atmos.,
678 107, 2002.
679 Stutz, J., Alicke, B., Ackermann, R., Geyer, A., Wang, S., White, A. B., Williams, E. J.,
680 Spicer, C. W., and Fast, J. D.: Relative humidity dependence of HONO chemistry in
681 urban areas, J. Geophys. Res.-Atmos., 109, D03307, 10.1029/2003JD004135, 2004.
682 Su, H.: HONO: a Study to its Sources and Impacts from Field Measurements at the Sub-urban
683 Areas of PRD Region, PhD Thesis of Peking University, 2008.
684 Su, H., Cheng, Y. F., Shao, M., Gao, D. F., Yu, Z. Y., Zeng, L. M., Slanina, J., Zhang, Y. H.,
685 and Wiedensohler, A.: Nitrous acid (HONO) and its daytime sources at a rural site
686 during the 2004 PRIDE-PRD experiment in China, J. Geophys. Res.-Atmos., 113,
687 D14312, 10.1029/2007jd009060, 2008.
688 Su, H., Cheng, Y., Oswald, R., Behrendt, T., Trebs, I., Meixner, F. X., Andreae, M. O., Cheng,
689 P., Zhang, Y., and Pöschl, U.: Soil Nitrite as a Source of Atmospheric HONO and OH
690 Radicals, Science, 333, 1616-1618, 10.1126/science.1207687, 2011.
691 Muller, Th., Dubois, R., Spindler, G., Bruggemann, E., Ackermann, R., Geyer, A., and Platf,
692 U.: Measurements of Nitrous Acid by DOAS and Diffusion Denuders: A Comparison,
693 Transactions on Ecology and the Environment, 28, ISSN 1743-3541, 1999.
694 VandenBoer, T. C., Brown, S. S., Murphy, J. G., Keene, W. C., Young, C. J., Pszenny, A. A.
695 P., Kim, S., Warneke, C., de Gouw, J. A., Maben, J. R., Wagner, N. L., Riedel, T. P.,
696 Thornton, J. A., Wolfe, D. E., Dubé, W. P., Öztürk, F., Brock, C. A., Grossberg, N.,
697 Lefer, B., Lerner, B., Middlebrook, A. M., and Roberts, J. M.: Understanding the role of
698 the ground surface in HONO vertical structure: High resolution vertical profiles during
699 NACHTT-11, J. Geophys. Res.-Atmos., 118, 10,155-110,171, 10.1002/jgrd.50721,

2013.

Veres, P., Roberts, J. M., Burling, I. R., Warneke, C., de Gouw, J., and Yokelson, R. J.: Measurements of gas-phase inorganic and organic acids from biomass fires by negative-ion proton-transfer chemical-ionization mass spectrometry, J. Geophys. Res.-Atmos., 115, D23302, 10.1029/2010jd014033, 2010.

Wang, S., Zhou, R., Zhao, H., Wang, Z., Chen, L., and Zhou, B.: Long-term observation of atmospheric nitrous acid (HONO) and its implication to local NO_2 levels in Shanghai, China, Atmos. Environ., 77, 718-724, 10.1016/j.atmosenv.2013.05.071, 2013.

Wang, T., Wong, C. H., Cheung, T. F., Blake, D. R., Arimoto, R., Baumann, K., Tang, J., Ding, G. A., Yu, X. M., Li, Y. S., Streets, D. G., and Simpson, I. J.: Relationships of trace gases and aerosols and the emission characteristics at Lin'an, a rural site in eastern China, during spring 2001, J. Geophys. Res.-Atmos., 109, D19S05, 10.1029/2003JD004119, 2004.

Xu, Z., Wang, T., Xue, L. K., Louie, P. K. K., Luk, C. W. Y., Gao, J., Wang, S. L., Chai, F. H., and Wang, W. X.: Evaluating the uncertainties of thermal catalytic conversion in measuring atmospheric nitrogen dioxide at four differently polluted sites in China, Atmos. Environ., 76, 221-226, 10.1016/j.atmosenv.2012.09.043, 2013.

Figure Captions:

Fig. 1 Temporal variation of the concentrations of HONO, NO_2 $PM_{2.5}$ mass and potassium, at the SORPES station during late April to June 2012. Biomass burning episodes were mostly occurred during late May and early June (shaded in the figure).

Fig. 2 Whisker plot of diurnal variation of (a) HONO and (b) HONO/NO_2 at the SORPES station during April to June 2012.

Fig. 3 Comparisons between biomass burning periods (203 samples) and non-biomass burning period (1122 samples) of (a) $PM_{2.5}$ concentrations, (b) concentrations of organic matters in $PM_{2.5}$ (estimated by $PM_{2.5}$-WSIs), (c) NO_2 concentrations, (d) HONO concentrations, (e) HONO to NO_2 ratio and (f) HONO to NO_x ratio. There are statistically significant differences for all the data pairs ($p<<0.01$) except NO_2 ($p=0.51$).

Fig. 4 Map of 8-hr Lagrangian backward retroplume (100 m footprint layer) for (a) biomass burning air masses (defined as $K^+ > 2$ ug m^{-3} and $K^+/PM > 2\%$) during night time, and (b) non-biomass burning air masses (defined as $K^+ < 2$ ug m^{-3} and $K^+/PM < 2\%$)and active fire (pink dots) during 1 June - 15 June, 2012 (Data obtained from FIRMS MODIS Fire Archive).

Fig. 5 Scatter plot between the HONO and potassium concentration during biomass burning periods

Fig. 6 Ratios of HONO to NO_2 for nighttime samples of BB (except of the June 10 case) and Non-BB plumes. The change rates were calculated from 19:00 to 02:59. Error bars are the standard deviations.

Fig. 7 (a) Scatter plot between the particle surface area and $PM_{2.5}$ for nighttime samples during BB and Non-BB periods, (b) Whisker plot of $PM_{2.5}$ in the selected mass concentration range (100–150μg m^{-3}, showed in Fig. 7a) during BB (51 samples) and Non-BB period (27 samples), and (c) particle surface area size distributions for the same subsets of data

Fig. 8 Scatter plot between the ratio of particle surface area to $PM_{2.5}$ and the abundance of potassium in $PM_{2.5}$ for nighttime samples during BB during BB period.

Fig. 9 Whisker plot of the ratios between $HONO/NO_2$ and particle surface area concentration for the samples at steady state (02:00-05:59) with the particle surface area in the range of $1.5–2.2 \times 10^{-9}$ m^2 cm^{-3} during the BB (14 samples) and non-BB periods (21 samples).

Fig. 10 Scatter plot between HONO and NO_2 concentration during the BB periods (without the case of 10^{th} June, blue solid squares), the beginning (red solid diamonds) and latter (green dots) state of the June 10^{th} episode.

Fig. 11 Whisker plots of (a) $PM_{2.5}$ mass, (b) ratios of HONO to NO_2, (c) ratios of $HONO/NO_2$ to $PM_{2.5}$ mass, (d) ratios of sulfate to $PM_{2.5}$, in the selected $PM_{2.5}$ mass concentration range (190 – 300 μg m^{-3}) in BB plume (10 samples) and the mixed plume (27 samples).

Fig. 12 Temporal variations of HONO, $HONO/NO_2$ ratios, RH, $PM_{2.5}$, sulfate in $PM_{2.5}$ and SO_2 during 9 - 11 June 2012 at the SORPES station

Fig. 13 Scatter plot between HONO and sulfate concentration in $PM_{2.5}$ during the nighttime on 10 June.

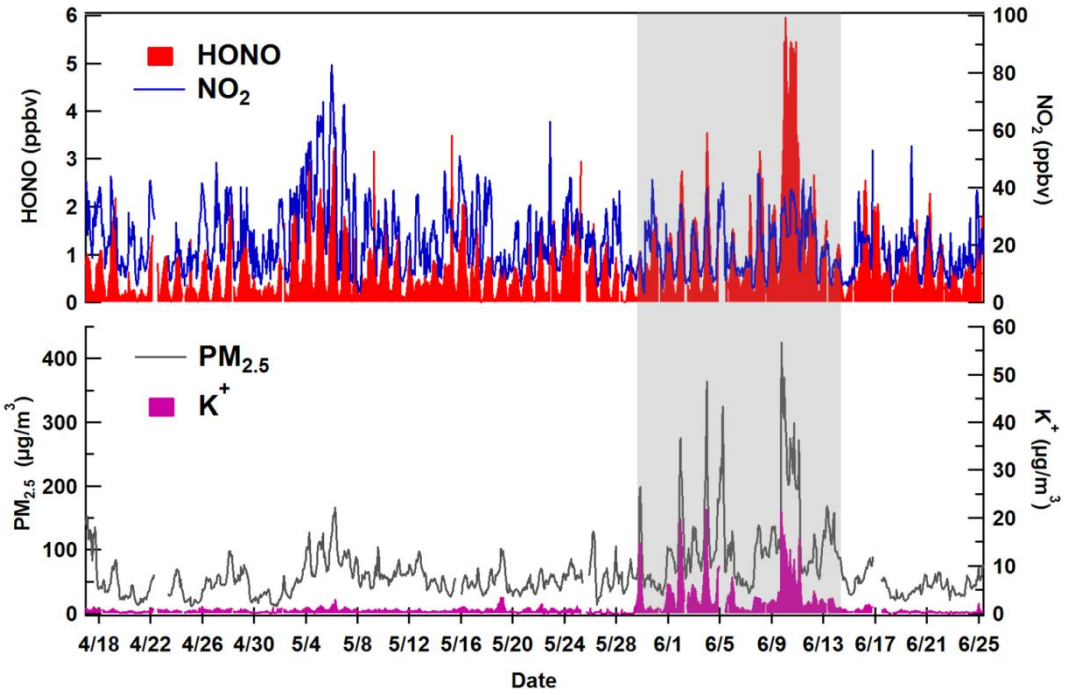

Fig. 1 Temporal variation of the concentrations of HONO, NO_2, $PM_{2.5}$ mass and potassium, at the SORPES central site during late April to June 2012. Biomass burning episodes were mostly occurred during late May and early June (shaded in the figure).

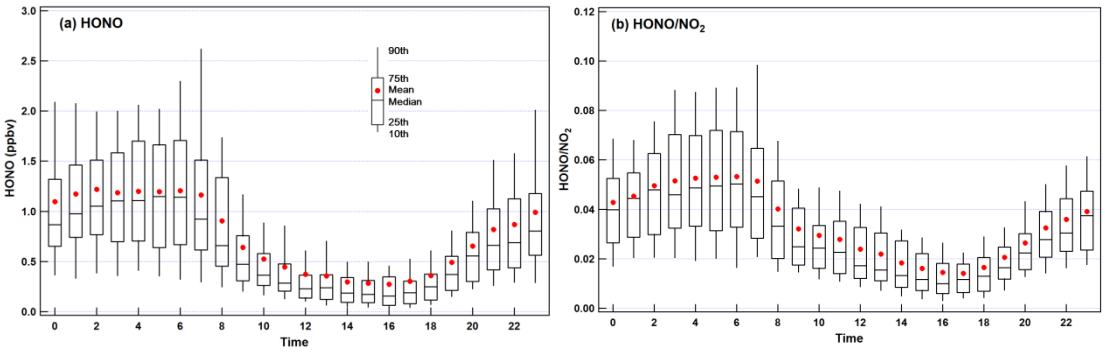

Fig. 2 Whisker plot of diurnal variation of (a) HONO and (b) $HONO/NO_2$ at the SORPES station during April to June 2012.

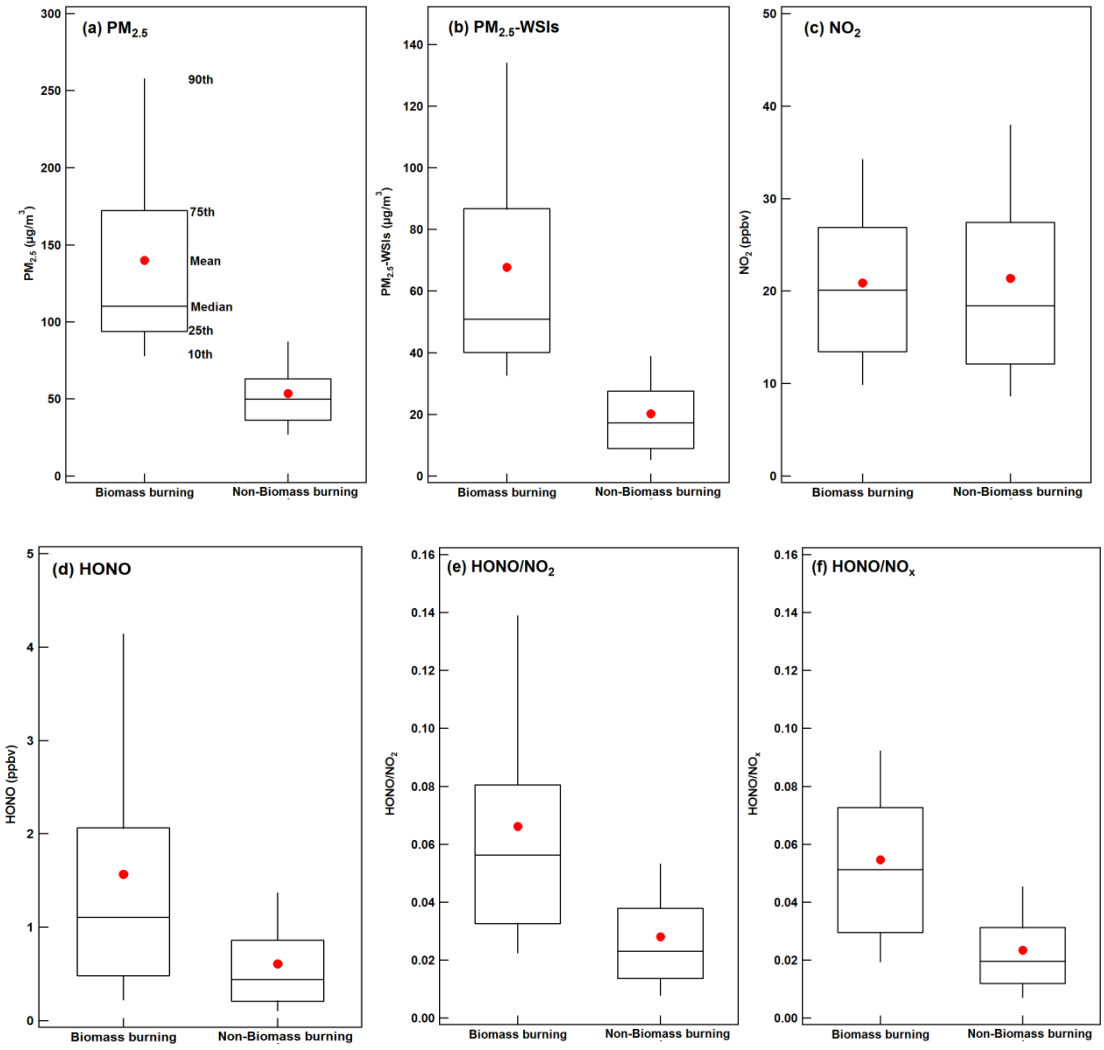

Fig. 3 Comparisons between biomass burning periods (1122 samples) and non-biomass burning period (203 samples) of (a) $PM_{2.5}$ concentrations, (b) concentrations of organic matters in $PM_{2.5}$ (estimated by $PM_{2.5}$-WSIs), (c) NO_2 concentrations, (d) HONO concentrations, (e) HONO to NO_2 ratio and (f) HONO to NO_x ratio. There are statistically significant differences for all the data pairs ($p<<0.01$) except NO_2 ($p=0.51$).

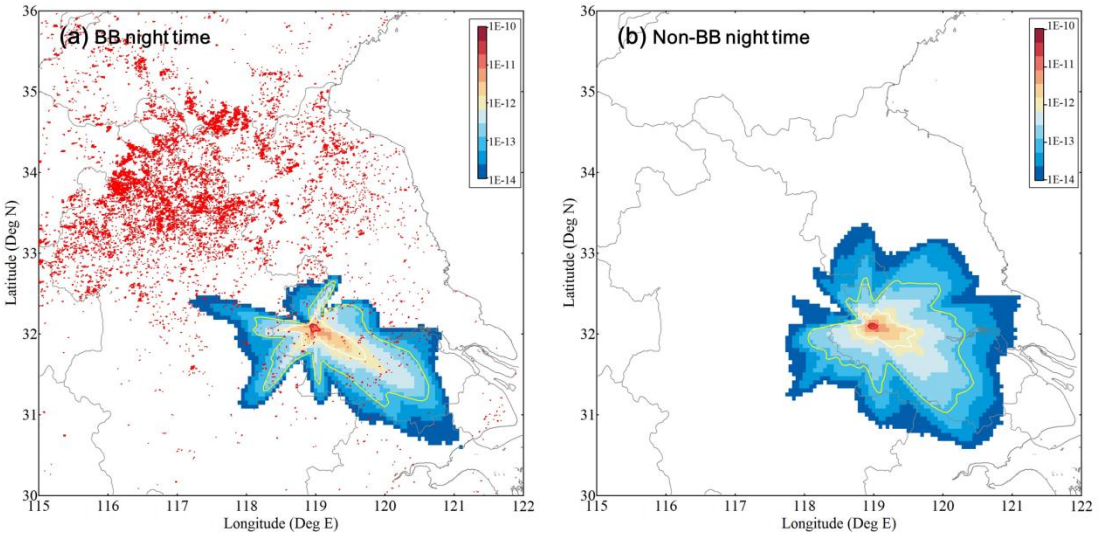

Fig. 4 Map of 8-hr Lagrangian backward retroplume (100 m footprint layer) for (a) biomass burning air masses (defined as $K^+ > 2$ ug m^{-3} and $K^+/PM > 2\%$) during night time, and (b) non-biomass burning air masses (defined as $K^+ < 2$ ug m^{-3} and $K^+/PM < 2\%$) and active fire (pink dots) during 1 June - 15 June, 2012 (Data obtained from FIRMS MODIS Fire Archive).

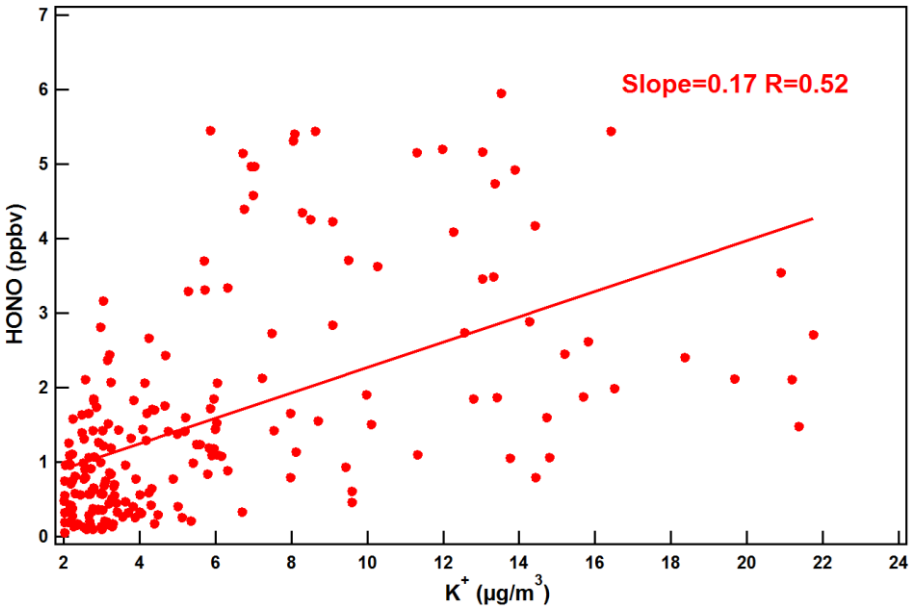

Fig. 5 Scatter plot between the HONO and potassium concentration during biomass burning periods.

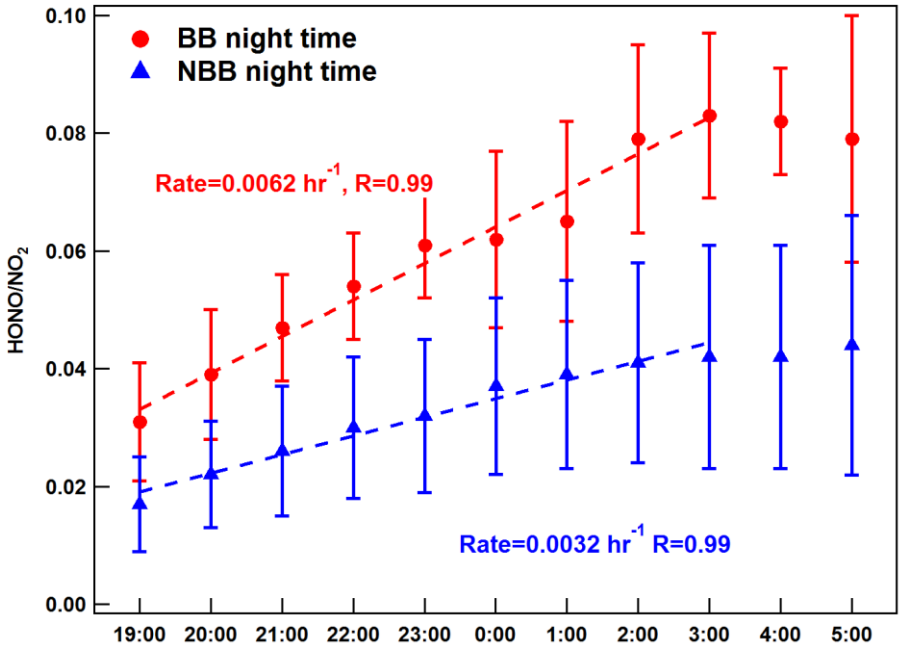

Fig. 6 Ratios of HONO to NO_2 for nighttime samples of BB (except of the June 10 case) and Non-BB plumes. The change rates were calculated from 19:00 to 03:00. Error bars are the standard deviations.

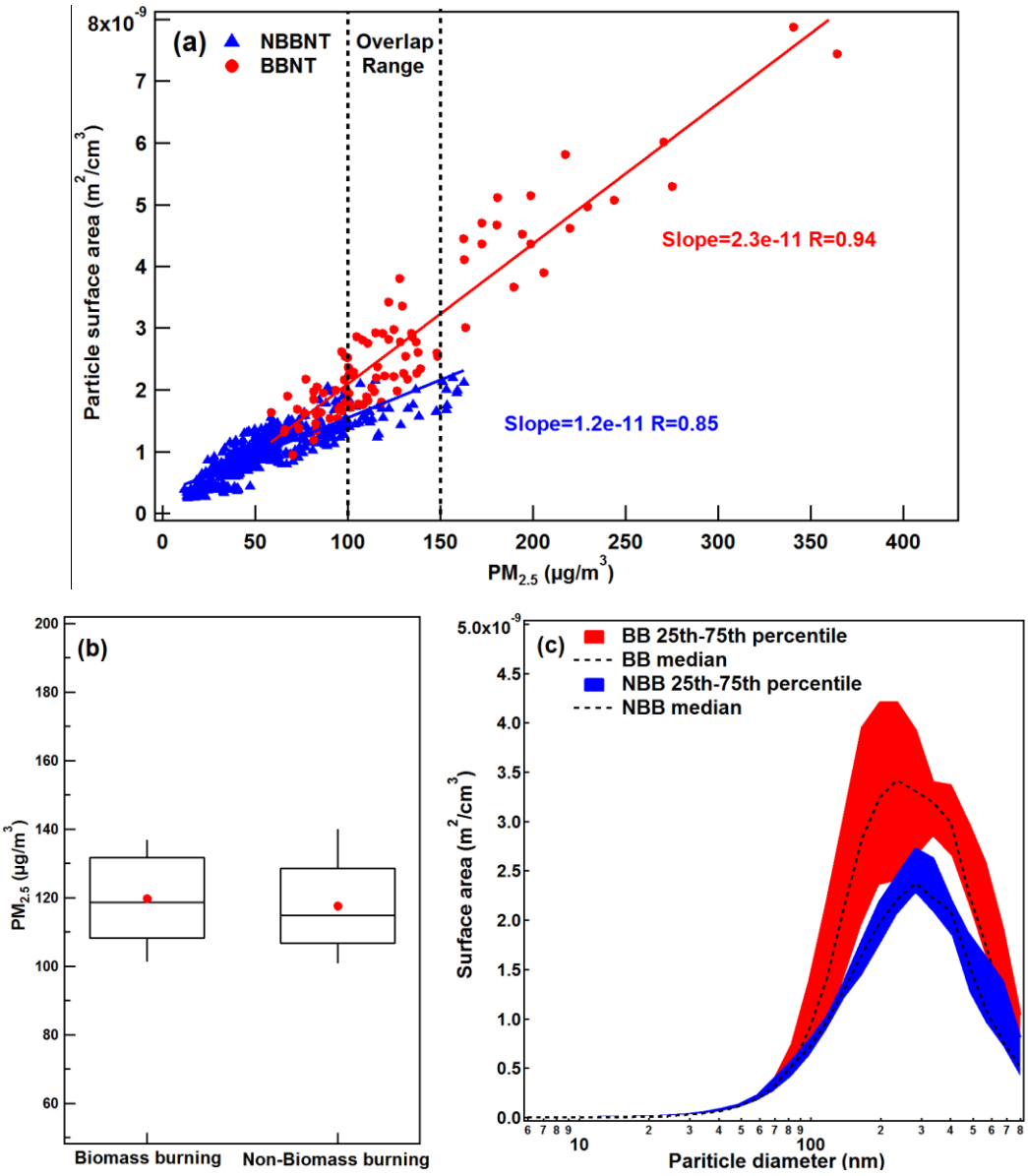

Fig. 7 (a) Scatter plot between the particle surface area and $PM_{2.5}$ for nighttime samples of BB and Non-BB plumes, (b) Whisker plot of $PM_{2.5}$ in the selected mass concentration range (100–150μg m^{-3}, showed in Fig. 7a) during BB (51 samples) and Non-BB period (27 samples), and (c) particle surface area size distributions for the same subsets of data.

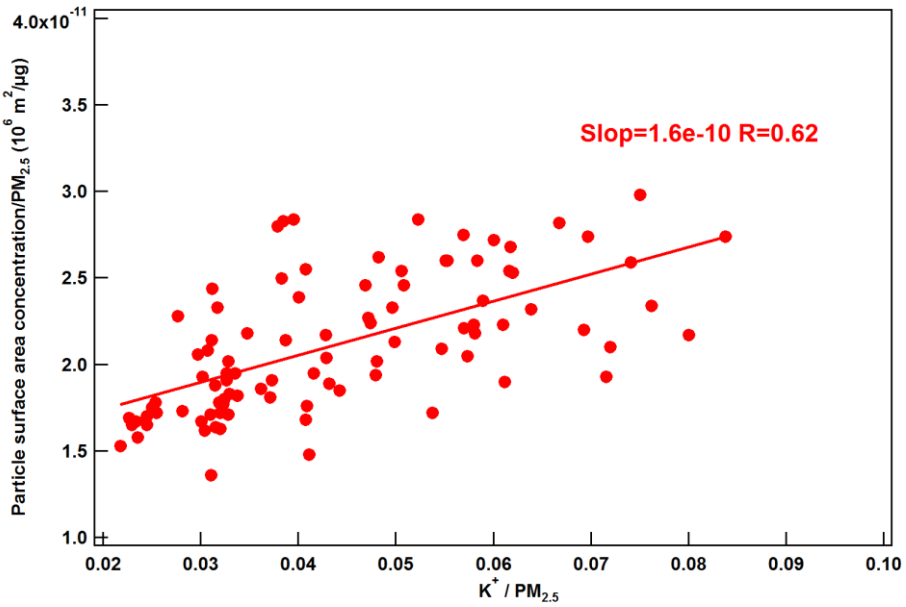

Fig. 8 Scatter plot between the ratio of particle surface area to $PM_{2.5}$ and the abundance of potassium in $PM_{2.5}$ for nighttime samples during BB during BB period.

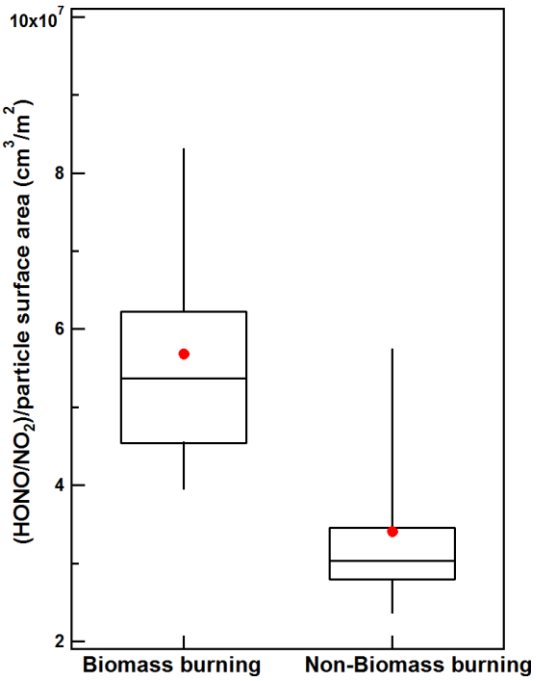

Fig. 9 Whisker plot of the ratios between $HONO/NO_2$ and particle surface area concentration for the samples at steady state (02:00-05:59) with the particle surface area in the range of $1.5–2.2 \times 10^{-9}$ m^2 cm^{-3} during the BB (14 samples) and non-BB periods (21 samples).

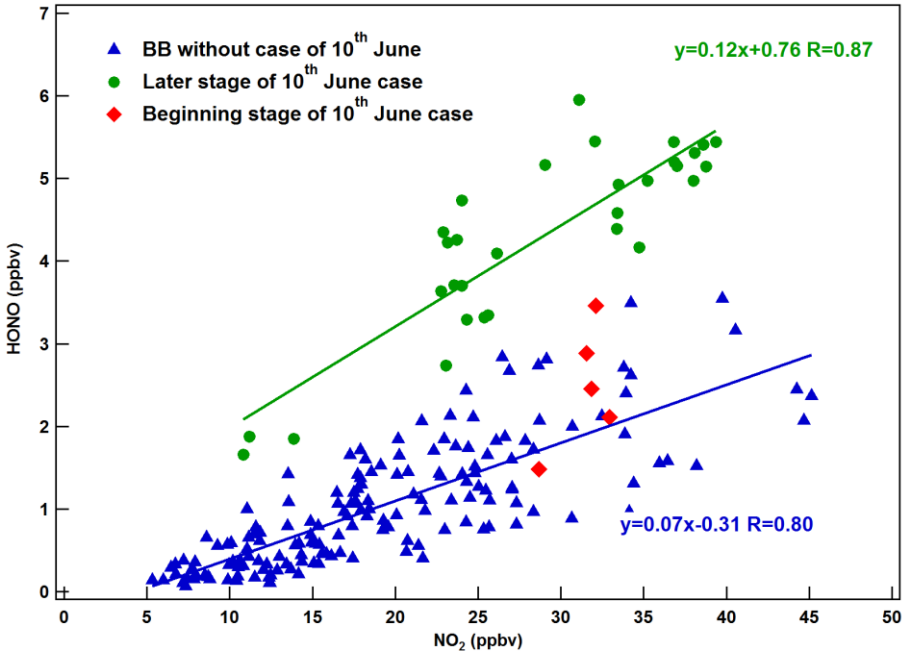

Fig. 10 Scatter plot between HONO and NO_2 concentration during the BB periods (without the case of 10th June, blue solid squares), the beginning (red solid diamonds) and latter (green dots) state of the June 10th episode.

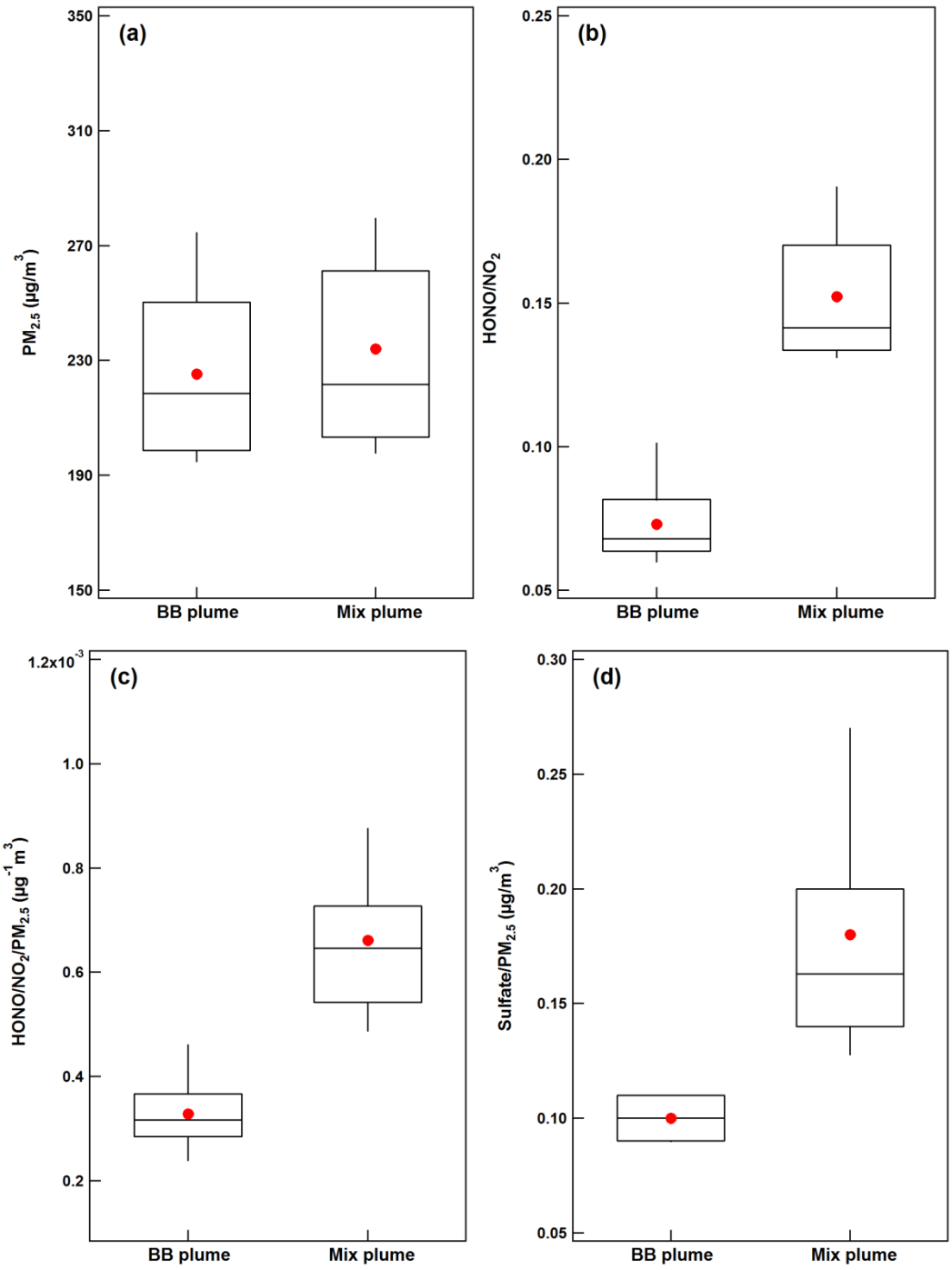

Fig. 11 Whisker plots of (a) $PM_{2.5}$ mass, (b) ratios of HONO to NO_2, (c) ratios of $HONO/NO_2$ to $PM_{2.5}$ mass, (d) ratios of sulfate to $PM_{2.5}$, in the selected $PM_{2.5}$ mass concentration range (190–300 μg m^{-3}) in BB plume (10 samples) and the mixed plume (27 samples).

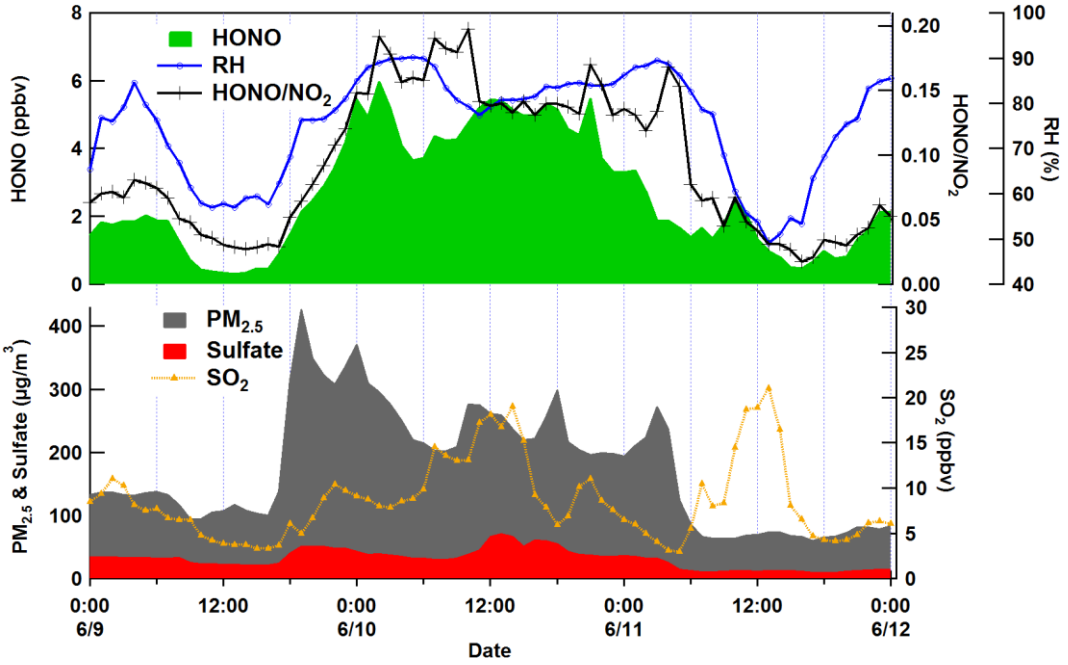

Fig. 12 Temporal variations of HONO, $HONO/NO_2$ ratios, RH, $PM_{2.5}$, sulfate in $PM_{2.5}$ and SO_2 during 9 - 11 June 2012 at the SORPES central site.

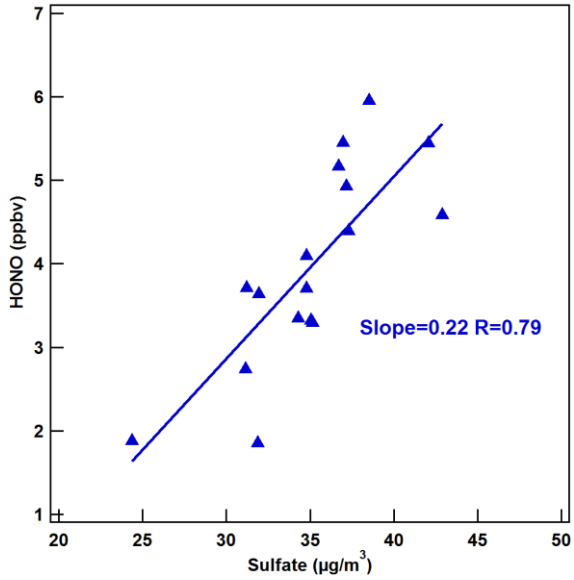

Fig. 13 Scatter plot between HONO and sulfate concentration in $PM_{2.5}$ during the nighttime on 10 June